Design of a 43kW Switched Reluctance Machine for a High-Performance Hybrid Electric Vehicle

*Ahmad Talha, Gaurang Vakil, Tom Cox, Chris Gerada**

**University of Nottingham, England, gaurang.vakil@nottingham.ac.uk*

Keywords: Finite Element Analysis, Hybrid Electric Vehicle, Reluctance Torque, Switched Reluctance Machine, Torque Ripple.

Abstract

A switched reluctance machine (SRM) is very robust and capable to perform well under harsh conditions. It is simple in construction and avoids the use of magnets so it is cheap to manufacture. The powertrain of a hybrid vehicle presents challenging conditions for an electric machine. A SRM is a potentially strong contender for such applications. In this paper, a 43kW SRM is designed for a hybrid traction application. Three topologies: three-phase 6/4, three-phase 12/8 and 4-phase 8/6 machines are considered as possible design choices. The main design objectives are to satisfy the torque and efficiency requirements and a secondary objective is to minimise the torque ripple. A base design is developed for each topology under consideration. The base designs are improved by carefully focusing on the impact of all important machine geometrical parameters such as rotor diameter, pole arcs and stator back-iron thickness on torque and efficiency. One design topology is selected and a detailed design optimization is carried out to maximize the efficiency. Results show that SRM can meet torque and efficiency requirements. The efficiency increases with the speed so SRM is better suited to high speed traction application especially where the high field weakening is required with low back EMF.

1 Introduction

With a candid eye on the future, sustainable transportation has gained deserved importance. The electric vehicle (EV), in long term, and hybrid electric vehicle (HEV), in the short term, provide a way to reduce the carbon emissions. At the heart of an EV lies an electric machine. The characteristics that allow an electric machine to better perform in an EV application are summarised in [1, 2] and some important ones are listed here for a quick reference:

- High torque density and high power density
- Wide constant speed range with high efficiency
- High performance and cost effective
- High reliability
- Space and weight constraints [3]

Several types of machines have been tried for an electric vehicle. Permanent magnet (PM) machines satisfy most of the technical requirements however the ever fluctuating cost of magnets is the constraining factor in their universal use for EV application [1, 4, 5].

Switched Reluctance Machine (SRM) has the potential to be a good alternative to PM machines. It is robust, simple in construction and performs well in harsh environment [1, 5, 6]. This paper presents the design procedure of a SRM for a hybrid electric vehicle and characterisation of the performance of the designed SRM. Infolytica's Motor Solve and MagNet are the software tools used for finite element analysis (FEA).

2 Design specifications

The design specifications of the proposed SRM are presented in Table 1:

Operating voltage range (V)	300-400 VDC
Peak power (kW)	≥85kW from 0-3000 rpm for ≤ 20s (@270 Nm)
Continuous power (kW)	≥43kW from 3000-7000 rpm (@137Nm)
Speed range (rpm)	3000-7000 rpm
Maximum efficiency (%)	>95% from 3000-7000 rpm
Peak current (A)	<350Arms
Continuous current (A)	<200Arms
Torque ripple (%)	≤10%
Motor diameter (mm)	270 mm
Stator length (mm)	180 mm
Stator cooling	Type: liquid

Table 1: Design specifications

3 Design calculations

Three SRM topologies were selected to meet these specifications. 3-phase 6/4, 3-phase 12/8 and 4-phase 8/6 are the design choices for the base design of the machine. 3-phase 6/4 offers the simplest solution however the torque ripple is expected to be higher. 3-phase 12/8 should produce lower torque ripple so better average torque. 4-phase 8/6 machine should give lower torque ripple, higher average at a lower commutation frequency than 3-phase 12/8 topology. However, the fourth phase shall make the drive more complex and expensive. Machines with higher pole numbers or phases have not been considered as higher pole numbers reduce the pole widths so inductance ratio decreases. Also, the commutation frequency is high which increases copper and core losses. Higher phase numbers would make drive expensive as already stated and would need more sophisticated control philosophy.

The design calculations for each of the topologies tested include calculation of geometric parameters such as rotor diameter, shaft diameter, rotor slot depth, stator slot depth, rotor pole arc, stator pole arcs, rotor pole width and stator pole width etc. The calculation of each of these parameters is based on the procedure described in and are used in as well.

All design calculations begin with the torque equation:

$$T = KD_r^2 L \tag{1}$$

Where D_r is rotor diameter, L is stack length and K is output coefficient. K represents the product of electric and magnetic loading and as suggested in [7], K should be determined based on FEA therefore in this project we begin by dimensioning the machine based on the method of [8] and then improve the design according to simulation results to get the required torque. The details of calculating each parameter follow this section.

3.1 Rotor diameter

T. Miller [8] has provided some recommended rotor diameter (D_r) to stator diameter (D_s) ratios for each of the topologies described above. The recommended ratios are tabulated in Table 2 and respective rotor diameters for each topology are calculated using these ratios.

	3-phase 6/4	3-phase 12/8	4-phase 8/6
D_r/D_s	0.5	0.53	0.57

Table 2: Recommended rotor diameter to stator diameter ratios.

3.2 Pole arcs and arc widths

Recommended pole arcs for selected topologies are provided in [8] and are listed in Table 3. The pole arcs are denoted by β_r and β_s for rotor and stator respectively. The pole widths are given by Equation (2) and Equation (3):

$$t_r = 2R_r \sin\frac{\beta_r}{2} \tag{2}$$

$$t_s = 2(R_r + g)\sin\frac{\beta_s}{2} \tag{3}$$

Where R_r is rotor radius and g is airgap length.

3.3 Yoke width

The yoke width should be at least half the pole width. There is a margin added as well to avoid localised saturation. The recommended value for the yoke width is 2/3 of respective pole width [8] i.e.

$$y_r = \frac{2}{3}t_r \tag{4}$$

$$y_s = \frac{2}{3}t_s \tag{5}$$

3.4 Slot depth

The rotor slot depth (d_r) is recommended in [8] to be one half of t_s. The stator slot depth (d_s) is calculated by the already calculated parameters. Higher slot depth increases slot area thereby allowing reduction in copper losses.

$$d_r = \frac{t_s}{2} \tag{6}$$

$$d_s = \frac{1}{2}\{D_s - D_r - 2(g + y_s)\} \tag{7}$$

3.5 Shaft diameter

By calculating rotor slot depth and rotor yoke width the shaft diameter (D_{sh}) is then given by the Equation (8):

$$D_{sh} = D_r - 2(d_r + y_r) \tag{8}$$

The shaft diameter should be made as large as possible to ensure mechanical integrity and increase the first critical speed [8].

3.6 Number of turns per phase

To calculate the approximate number of turns, assume that at certain speed the conduction angle for the transistors is equal to the step angle. Assuming the linear increase in flux linkage we can write:

$$\psi = \frac{V}{\omega}\varepsilon \tag{9}$$

Where V is the rated voltage, ω is rated speed and ε is step angle. We can also write the equation for flux linkage in terms of flux density and number of turns per phase as:

$$\psi = t_s L B_s n_c N_p \tag{10}$$

Where t_s is stator pole width, L is stack length, B_s is maximum flux density, n_c is number of coils per phase and N_p is number of turns per phase. Equating Equation (9) and Equation (10) we get,

$$\frac{V}{\varepsilon}\omega = t_s L B_s n_c N_p$$

Rearranging gives,

$$N_p = \frac{V\varepsilon}{\omega t_s L B_s n_c} \quad (11)$$

All calculated parameters for the selected designs are listed in Table 3.

Parameter	Design Topology					
	3-Phase 6/4		3-Phase 12/8		4-Phase 8/6	
Rotor diameter (mm)	135		143.1		153.9	
Pole arcs (deg)	32°	30°	16°	15°	23°	21°
Pole widths (mm)	37.21	35.46	21.42	20.35	28.53	26.44
Yoke widths (mm)	24.81	23.64	14.28	13.57	19.02	17.63
Slot depths (mm)	17.73	42.86	10.17	43.48	13.22	44.82
Shaft diameter (mm)	49.93		104.99		78.62	
Number of turns per phase	40		35		27	

Table 3: Calculated parameters for the considered design topologies

4 Preliminary simulations

Based on the calculations for each design, simulations were performed for each topology to get the base performance. The material used for stator and rotor core is M300-35A. Epoxy resin is used as slot liner material and winding fill factor is set at 0.5. For easy referencing, 3-phase 6/4 design will be designated as D-1, 3-phase 12/8 design as D-2 and 4-phase 8/6 as D-3 in this text from this point onwards. The results obtained with base designs are tabulated in Table 4.

Parameters	Designs		
	3-phase 6/4	3-phase 12/8	4-phase 8/6
Torque (Nm)	132	108	105
Input power (kW)	48.1	39.2	35.8
Output power (kW)	41.5	33.9	32.9
Efficiency (%)	86.3	86.4	92
Total losses (kW)	6.58	5.3	2.85

Table 4: Comparison of preliminary simulation results

5 Design optimisation

As evident through the preliminary simulation, the proposed designs, in particular D-2 and D-3 need improvement. Considering the specifications for this project, the key goal is recognised as to obtain the required torque with the required efficiency. Therefore, during each step of the design improvement, the values of the parameters are selected to give the best combination of torque and efficiency. As a secondary part of sensitivity analysis, effect of each parameter variation on the torque ripple is also graphically presented. The data related to torque ripple variation would enable us to identify the parameters that need to be optimised for torque ripple minimisation.

Rather than looking at variation of all important parameters such as rotor diameter, stator and rotor pole arcs, stator core thickness etc. altogether on the characteristics of the machine, here a simplistic approach is adopted. All parameters are changed one by one while keeping other parameters fixed except for the case of rotor diameter. The effect of changing each parameter individually on the overall design is predictable to certain extent hence probability of false optimums is low. At the end of the improvement process, one design out of these three will be selected based on the generated results.

The improvement process begins with choosing rotor and shaft diameters by simulating for a range of their values. The other parameters are calculated in this step as changing the rotor and shaft diameters changes other parameters anyways so by calculating the other parameters, the change is controlled. After the diameters, pole arcs and skewing angles for poles are chosen. End-turn overhang length should be kept in proportion to the stator pole arc as suggested in [8] so in case of D-1 design the pole arcs are kept to default values as increasing the stator pole arc means that end-turn length can increase beyond the length of stator itself. Skewing the poles should help in better focusing the flux from one pole to another. After pole arcs, stator pole depth and rotor core thickness are also optimised. Lastly coil size is selected to occupy the maximum of available slot area. A little exception in case of design D-2 is that before beginning the improvement process, number of turns in stator coil were reduced to lower the inductance and allow the current to reach its rated value.

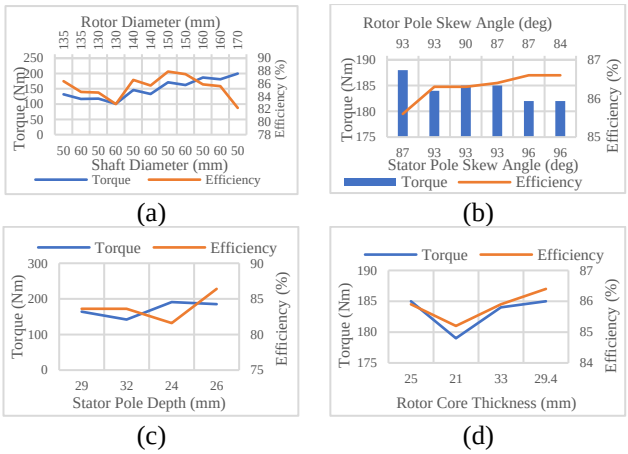

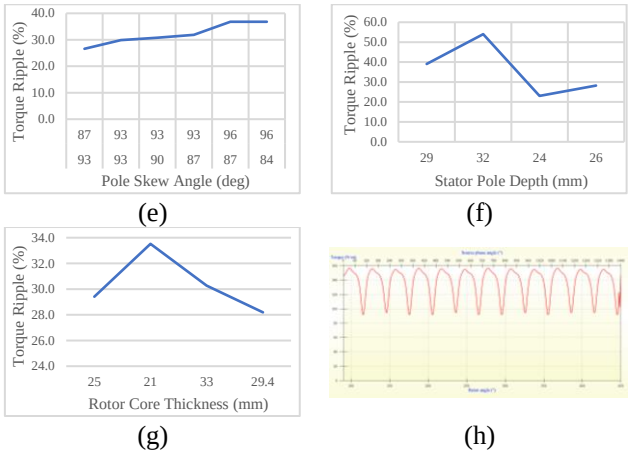

Figure 1: Improvement process for D-1.
(a)-(d): Torque and efficiency vs. rotor and shaft diameters, poles skew angles, stator pole depth and rotor core thickness respectively.
(e)-(g): Torque ripple vs. pole skew angles, stator pole depth and rotor core thickness respectively.
(h) Torque waveform of D-1

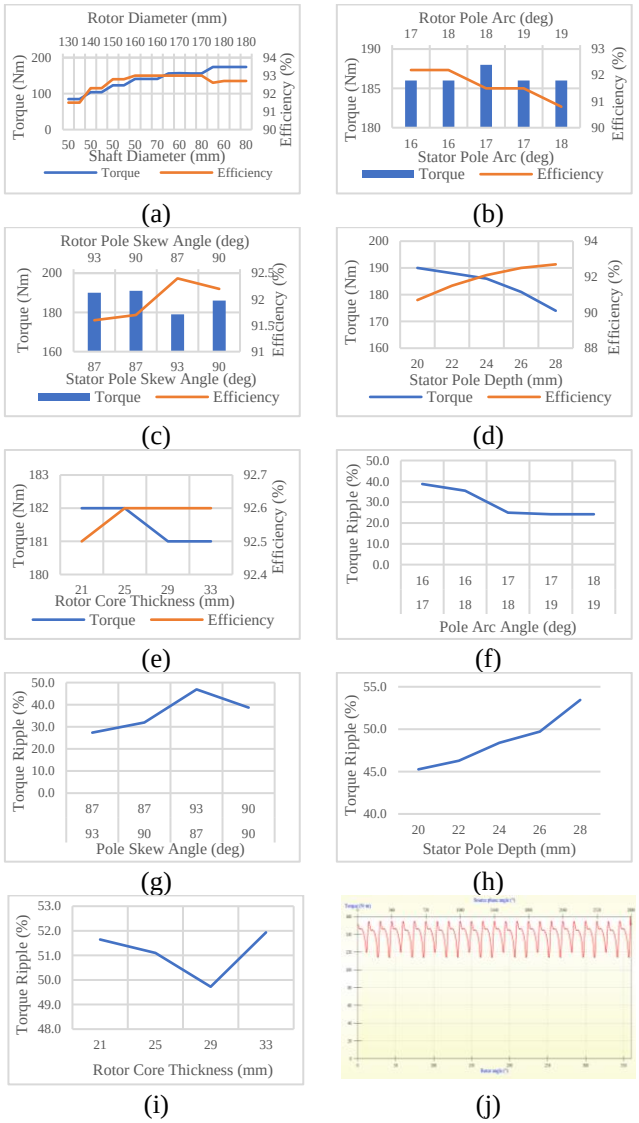

Figure 2: Improvement process for D-2.

(a)-(e): Torque and efficiency vs. rotor and shaft diameters, poles arcs and skew angles, stator pole depth and rotor core thickness respectively.
(f)-(i): Torque ripple vs. pole arcs and skew angles, stator pole depth and rotor core thickness respectively.
(j) Torque waveform of D-2

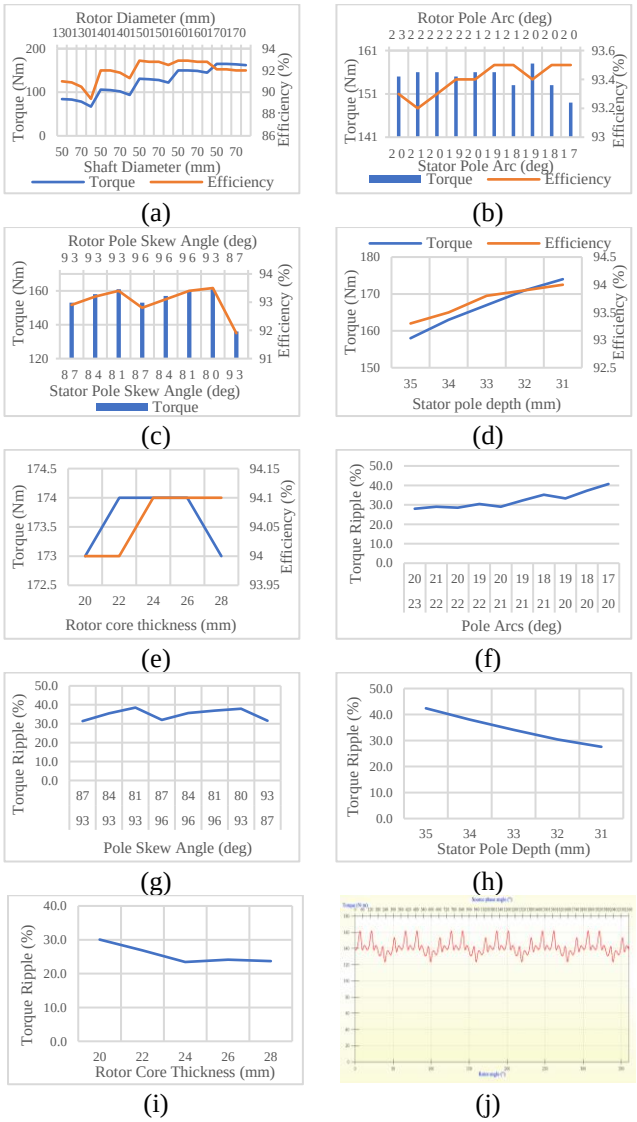

Figure 3: Improvement process for D-3
(a)-(e): Torque and efficiency vs. rotor and shaft diameters, poles arcs and skew angles, stator pole depth and rotor core thickness respectively.
(f)-(i): Torque ripple vs. pole arcs and skew angles, stator pole depth and rotor core thickness respectively.
(j) Torque waveform of D-3

Figure 1, Figure 2 and Figure 3 present the various stages of the improvement process for the respective design. Based on the results, values maximising the performance were selected. The chosen geometrical values are tabulated in Table 5 and the results are presented in Table 6. All machines were capable to produce much more than rated torque with rated current so the current was reduced to get rated torque at a higher efficiency. The next step is to choose the design which offers the best performance considering the specifications for this project.

Parameters	Designs		
	D-1	D-2	D-3
Rotor diameter (mm)	160	180	160
Shaft diameter (mm)	50	60	60
Stator pole arc (deg)	30	16	19
Rotor pole arcs (deg)	32	17	20
Stator pole depth (mm)	26	26	31
Rotor core thickness (mm)	29.4	25	26

Table 5: Chosen values for simulated variables in the improvement process

Parameters	Designs		
	D-1	D-2	D-3
Torque (Nm)	137	139	141
Input power (kW)	46.4	46.1	46.9
Output power (kW)	43	43.5	44.4
Efficiency (%)	92.8	94.3	94.7
Total losses (kW)	3.4	2.6	2.48
Current for rated torque (% of rated current)	98%	77%	80%

Table 6: Comparison of simulation results after improvement

5.1 Final selection of design

D-2 design has been chosen as the design suitable for this application. It offers higher efficiencies at lower speeds, has low torque ripple and requires the three-phase drive. Although D-3 offers highest efficiency and lowest torque ripple at higher speeds, however, it would require an extra leg in the converter which would make the converter more expensive and the drive more complex. D-1 offers the lowest efficiencies among all designs throughout the speed range and has the highest torque ripple. Figure 4 and Figure 5 provide a comparison of torque-speed profiles and efficiencies of the considered design.

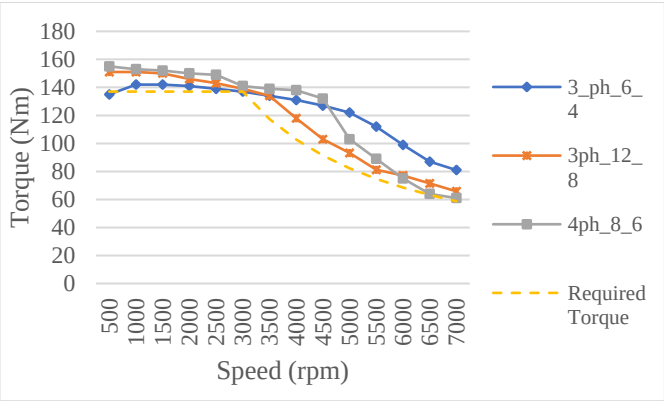

Figure 4: Torque-speed profiles of the considered designs

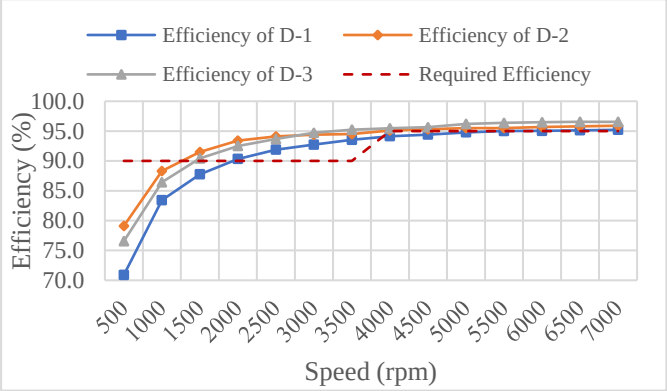

Figure 5: Comparison of efficiencies of D-1, D-2 and D-3 in the considered speed range

6 Performance characterisation of the selected design

6.1 Thermal analysis

Thermal analysis is an important part of machine design so that the efficiency of heat removal process from the machine can be determined. Thermal modelling depicts the behaviour of the system with respect to heat distribution and heat removal considering the geometry of the machine [9] MotorCAD was used for carrying out thermal analysis on the selected design. MotorCAD uses lumped circuits for the thermal analysis of a machine [10]. Simulations show that without using the liquid cooling the winding hot spot temperature exceeds 180°C which is maximum temperature allowed for insulation class H [11]. Therefore, liquid cooling was added in form of a water jacket outside the stator. The cooling liquid used was water and the liquid flow rate was set as 12 litre/min. This gave winding hot spot temperature as 179°C which is permissible. Figure 6 shows thermal analysis result with maximum temperatures in different parts of the machine displayed.

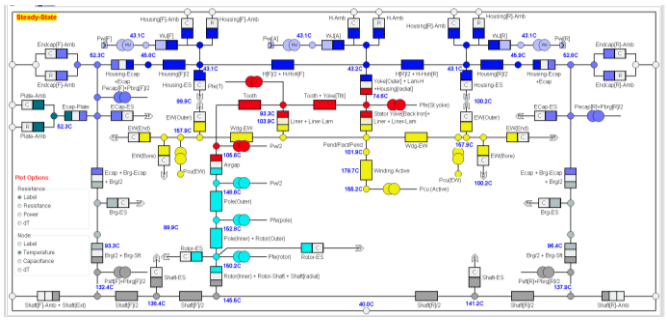

Figure 6: Thermal analysis results with 12 litre/min flow rate

6.2 Efficiency map

An efficiency map provides efficiency curves plotted over the torque-speed profile of a machine. It gives information about the efficiency of the machine at different power levels throughout the speed range under consideration. To build an efficiency map for the selected SRM, torque-speed profiles were developed at different current levels. Current levels used were 100%, 77% (value of the current used to get rated power),

50% and 20% of the rated value of current. To develop torque-speed profile, the turn-on and turn-off angles were advanced with the speed. The optimum values of these angles were found by repeated simulations. Figure 7 presents the developed efficiency map for the designed machine.

6.3 Finite element analysis

Finite element analysis was performed to verify the magnetic flux density levels in the stator and rotor core. As SRM needs to operate in saturation region, it must be noted that high saturation of stator and rotor core would hinder the performance of the machine. The peak flux density occurs at the pole corners due to localised saturation. The flux density in the stator back iron and rotor iron is much less which bodes well for the design (refer to Figure 8).

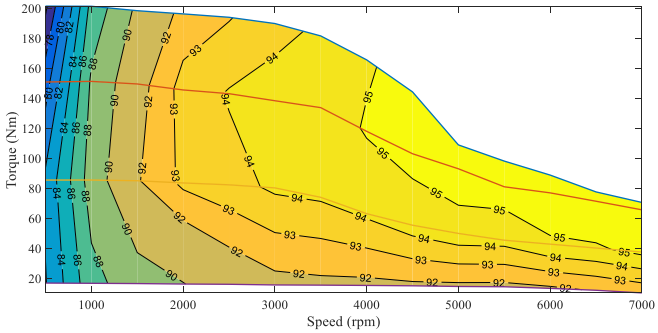

Figure 7: Efficiency map of the selected SRM

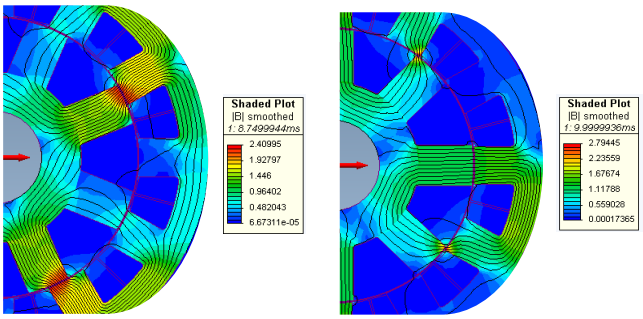

(a) (b)

Figure 8: Magnetic field density distribution when:
(a) Phase A is unaligned
(b) Phase A is aligned

7 Conclusions

This paper presents a detailed procedure for designing a switched reluctance machine for the given specifications for hybrid electric vehicle application. The results endorse that switched reluctance machine can be a capable replacement to permanent magnet machines. It meets the important specifications however falls short of satisfying the torque ripple criteria. Given the advantages it offers, the only compromise is the complex control system it needs for its optimum performance.

References

[1] E. Bostanci, M. Moallem, A. Parsapour and B. Fahimi, "Opportunities and Challenges of Switched Reluctance Motor Drives for Electric Propulsion: A Comparative Study," *IEEE Transactions on Transportation Electrification*, vol. 3, no. 1, pp. 58-75, 2017.

[2] K. Chau and W. Li, "Overview of electric machines for electric and hybrid vehicle," *International Journal of Vehicle Design,*, vol. 64, no. 1, pp. 46-71, 2014.

[3] T. Finken, M. Felden and K. Harmeyer, "Comparison and design of different electrical machine types regarding their applicability in hybrid electrical vehicles," in *Proc. 18th International Conference on Electrical Machines*, Vilamoura, 2008.

[4] D. Ronanki and S. S. Williamson, "Comparative analysis of DITC and DTFC of switched reluctance motor for EV applications," in *2017 IEEE International Conference on Industrial Technology (ICIT)*, Toronto, 2017.

[5] J. W. Jiang, B. Bilgin and A. Emadi, "Three-Phase 24/16 Switched Reluctance Machine for a Hybrid Electric Powertrain," *IEEE Transactions on Transportation Electrification*, vol. 3, no. 1, pp. 76-85, 2017.

[6] C. Mi, M. A. Masrur and D. W. Gao, Hybrid Electric Vehicles: Principles and Applications with Practical Perspectives, Sussex: John Wiley & Sons Ltd., 2011.

[7] P. Rafajdus, A. Peniak, D. Peter, P. Makyś and L. Szabó, "Optimization of switched reluctance motor design procedure for electrical vehicles," in *2014 International Conference on Optimization of Electrical and Electronic Equipment (OPTIM)*, Bran, 2014.

[8] T. Miller, Switched Reluctance Motors And Their Control, Magna Physics Publishing, 1993.

[9] B. Anderson, "Lumped Parameter Thermal Modelling of Electric Machines," 2013. [Online]. Available: http://publications.lib.chalmers.se/records/fulltext/185192/185192.pdf. [Accessed 10 September 2017].

[10] D. Staton, D. Hawkins and M. Popescu, "Motor-CAD Software for Thermal Analysis of Electrical Motors - Links to Electromagnetic and Drive Simulation Models," [Online]. Available: https://www.motor-design.com/wp-content/uploads/2016/12/cwieme_2010_paper_mdl.pdf. [Accessed 10 September 2017].

[11] The Association of Electrical & Mechanical Trades, "Classification of Insulation Systems," 2014. [Online]. Available: http://www.theaemt.com/technical-info/general-engineering/classification-of-insulation-systems. [Accessed 22 August 2017].